Accepted Manuscript

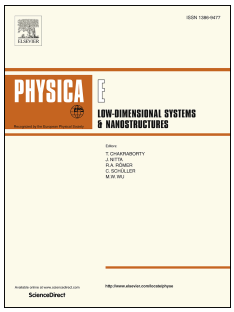

Stability of direct band gap under mechanical strains for monolayer MoS_2, $MoSe_2$, WS_2 and WSe_2

Shuo Deng, Lijie Li, Min Li

PII: S1386-9477(18)30240-6

DOI: 10.1016/j.physe.2018.03.016

Reference: PHYSE 13082

To appear in: *Physica E: Low-dimensional Systems and Nanostructures*

Received Date: 13 February 2018

Revised Date: 6 March 2018

Accepted Date: 12 March 2018

Please cite this article as: S. Deng, L. Li, M. Li, Stability of direct band gap under mechanical strains for monolayer MoS_2, $MoSe_2$, WS_2 and WSe_2, *Physica E: Low-dimensional Systems and Nanostructures* (2018), doi: 10.1016/j.physe.2018.03.016.

Shuo Deng[a], Lijie Li[b*], and Min Li[c]

[a] School of Logistics Engineering, Wuhan University of Technology, Wuhan, 430070, China.
[b] Multidisciplinary Nanotechnology Centre, College of Engineering, Swansea University, Swansea, SA1 8EN, UK.
[c] Department of Physics, Wuhan University of Technology, Wuhan, 430070, China.
* corresponding email: lijie.li@hotmail.co.uk

Abstract

Single layer transition-metal dichalcogenides materials (MoS_2, $MoSe_2$, WS_2 and WSe_2) are investigated using the first-principles method with the emphasis on their responses to mechanical strains. All these materials display the direct band gap under a certain range of strains from compressive to tensile (stable range). We have found that this stable range is different for these materials. Through studying on their mechanical properties again using the first-principles approach, it is unveiled that this stable strain range is determined by the Young's modulus. More analysis on strains induced electronic band gap properties have also been conducted.

Keywords: direct band gap; 2D materials; elastic properties; first principles.

1 Introduction

The transition-metal dichalcogenides (TMDs), such as MoS_2, $MoSe_2$, WS_2 and WSe_2 have attracted much attention owing to their superior electronic, optical, mechanical and catalytic properties [1-8]. It has been found that the monolayer TX_2 type (*T*, transition-metal atom; *X*, chalcogen atom) have several distinctive electronic and optical properties including a direct band gap (the band gap is in the range of 1.1 to 2.0 eV) at the *K* point in the Brillouin zone [9-11], strong photoluminescence effects[12-15] and the possibility of full optical control of the valley and spin occupation[16-19]. These properties will significantly enhance the potential of using them in various applications such as pressure sensors[20], fast photodetection[21], and nanoelectromechanical systems (NEMS) devices[22].

monolayer TX_2 changes from direct type to indirect type, more specifically the band gap has been narrowed, eventually leading to the CBM (conduction band minimum) plunge to below the Fermi level, which implicates that the material becomes exhibiting metal properties. Applying mechanical strains is one of the most promising ways to tune the band gap of the monolayer TX_2. However, a few theoretical groups reported the relationship between the Young's modulus and the deformation region of direct band gap[26, 29]. The study on the directional dependence of the mechanical strain has not been conducted so far[11, 26]. Hence the critical issue is to conduct a thorough investigation to unveil the relation between their mechanical properties and electronic properties.

In this work, we simulate the Young's modulus of monolayer TX_2 cells and investigate the band structures of hexagonal and orthorhombic monolayer TX_2 cells under a wide range of strain amplitudes in different directions using first-principles methods. This theoretical method has been used in many previous studies in TMDs[23-27]. Our aim is to theoretically explore the relationship between the Young's modulus and the width of the direct band gap region. Furthermore, the directional properties of strains acting on the orthorhombic monolayer TX_2 cells will also be explored. The effect of Young's modulus and various directions of strains on the monolayer TX_2 will be detailed in the following sections of this paper. The phonon spectral properties of these four materials have been studied in reference [11], and our focus was not on studying this property. We also neglect other properties which could be extracted from DFT, as it was simulated, for examples, in references [30, 31] for similar zigzag sheet monolayers with high Young's modulus and strong mechanical anisotropy.

2 Computational method

We start modelling the monolayer TX_2. By creating two types of crystal cells using the Atomistix ToolKit (ATK)[32] simulation tools, the lattice constants and key bond lengths/angles calculated are listed in Table 1. Based on the lattice constant of Table 1, the initial model of monolayer TX_2 are established. Shown in the Figure 1, the monolayer TX_2 can be viewed as composed of two-dimensional (2D) *X*-*T*-*X* sheets stacked on top of one

Table 1. Lattice parameters of monolayer TX_2

Material	a(Å)	d(Å)	θ(Å)
MoS_2	3.160	2.440	80.165
$MoSe_2$	3.288	2.524	82.477
WS_2	3.160	2.450	80.452
WSe_2	3.290	2.531	82.749

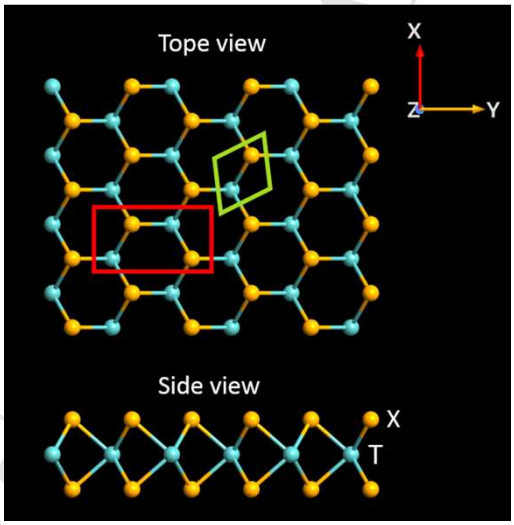

Figure 1. Schematic graphs of the 2D monolayer TX_2 type cells. The x and y lattice vectors are shown. The hexagonal (green) and orthorhombic (red) unite cells are indicated.

The band structures of the monolayer TX_2 type cells are calculated by the density functional theory (DFT) using the ATK. In our DFT calculation, we use a numerical Linear Combination of Atomic Orbitals (LCAO) basis sets, where the method was described in [33]. We use the generalized gradient approximation (GGA) with the parametrization of Perdew-

conditions. In order to optimize the geometries, we have utilized the Limited-memory Broyden Fletcher Goldfarb Shanno (LBFGS) algorithm[35] with the maximum stress tolerance value of 0.01 eV/Å^3. The structure is fully relaxed until the force on each atom becomes smaller than 0.01 eV/Å. Show in the Figure 2, for the hexagonal cell, in order to maintain the crystal symmetry, the biaxial symmetrical strains ε have to be applied in both the *x/y* plane. However, for the orthorhombic cell, we can apply biaxial asymmetric strains along the armchair (ε_a) and zigzag (ε_z) directions within the *x/y* plane. The deformation is simulated by setting the lattice parameter to a fixed larger value and relaxing the atomic positions. The amplitude of deformation is defined as: $\varepsilon = (a - a_0)/a_0$, where a_0 and a are the lattice parameters of the unstrained and strained cells, respectively.

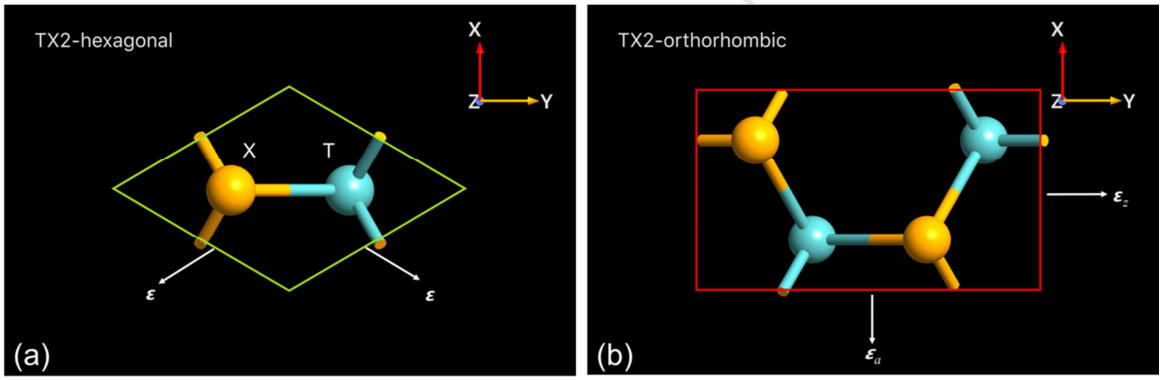

Figure 2. The applied strains directions are indicated by white arrows. (a) Symmetrical biaxial strains on the hexagonal cell. (b) Asymmetrical biaxial strains on the orthorhombic cell.

Using the DFT-GGA calculations, we show that the band gap (E_g) of the monolayer MoS_2, $MoSe_2$, WS_2 and WSe_2 are 1.76 eV, 1.43 eV, 1.95 eV and 1.62 eV, which are very close to recent DFT calculations[11, 13, 36, 37], but slightly smaller than that measured using complementary techniques of optical absorption, photoluminescence and photoconductivity of monolayer TX_2[11, 15]. Although the PBE exchange correlation functional in DFT underestimates the band gap, the GLLB-Sc and hybrid functional lead to better agreement with experiments. This trend is not generalized, and more often depends on the material and

by approximately 1 eV and 0.45 eV, respectively[38, 39]. Moreover, Ataca *et al* also reported a higher value of the band gap by use G_0W_0 (2.78 eV) and GW_0 (2.50 eV)[38]. Analyzing the aforementioned data, we believe that our choice of the PBE exchange correlation functional for monolayer MoS_2, $MoSe_2$, WS_2 and WSe_2 is appropriate.

3 Simulation results and discussion

We calculated band structures for various amplitudes of biaxial symmetric compressive and tensile strains on the monolayer TX_2 hexagonal cell, as show in Figure 3 and Figure 4, respectively. The bold black lines are the band when no strain is applied. At equilibrium, the monolayer TX_2 are direct band gap semiconductors with the conduction band minimum (CBM) and valence band maximum (VBM) at *K* point. Under strains (Figure 3 and Figure 4), the conduction band is decreasing and the valence band is increasing as the value of strains increase. The band structures have also changed from a direct band gap to an indirect band gap. The electronic states near the CBM and VBM contributed mainly from d_{z^2}, $d_{x^2-y^2}$ and d_{xy} orbitals of the *T* atom (Mo and W) and the p orbitals of the *X* atom (S and Se)[11]. The strong coupling between p orbitals of the *X* atom and $d_{xz} + d_{yz}$ orbitals of the *T* atom leads to a large splitting between their bonding and antibonding states, which influence the strain-induced band structures.

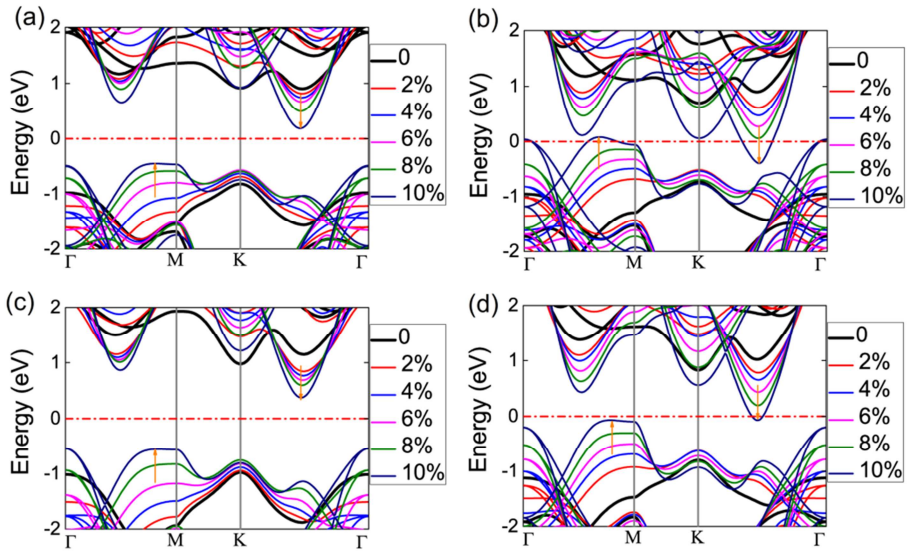

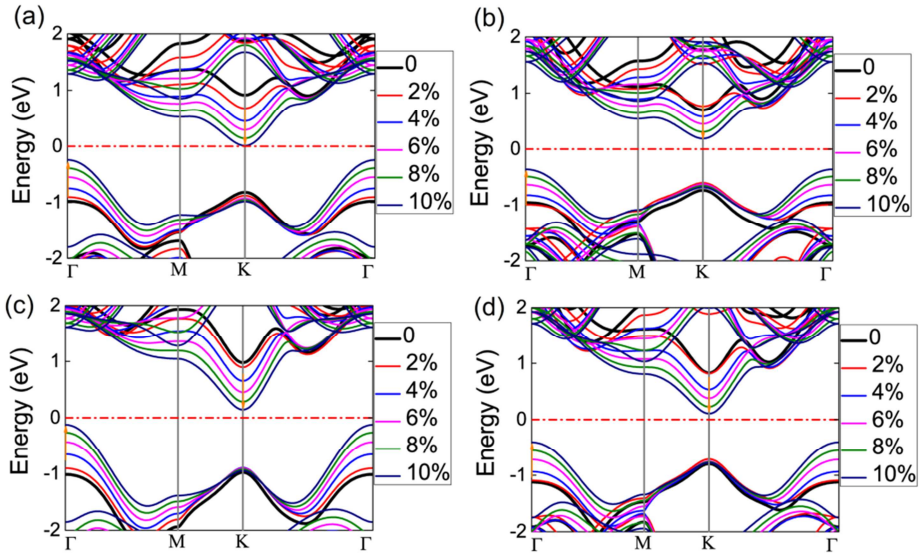

Figure 4. Band structures of monolayer MoS_2 (a), $MoSe_2$ (b), WS_2 (c) and WSe_2 (d) corresponding to 0%, 2%, 4%, 6%, 8%, 10% symmetrical biaxial tensile strains, respectively. The shift trend of the CBM and VBM are indicated by orange arrows.

In equilibrium, the monolayer TX_2 are direct band gap semiconductors with the CBM and VBM at the *K* point. Figure 5 shows the CBM evolution with the applied symmetrical biaxial strains for monolayer TX_2 hexagonal cells into three regimes. (1) In the central regime, monolayer TX_2 retains direct bang gap. The deformation ranges ($\Delta\varepsilon$) in which the materials remain in the direct band gap region (R_d) of the CBM-strain curves are 0.04, 0.08, 0.02 and 0.06 for monolayer MoS_2, $MoSe_2$, WS_2 and WSe_2, respectively. It is deduced that $R_{d\text{-}WS2}<R_{d\text{-}MoS2}<R_{d\text{-}WSe2}<R_{d\text{-}MoSe2}$. (2) Exceeding gray dashed lines, the tensile and compressive strains turn monolayer TX_2 into indirect band gap semiconductors and the amplitude of the CBM keep decline. (3) Under red dot chain line, the compressive strains turn the CBM lower than 0 eV.

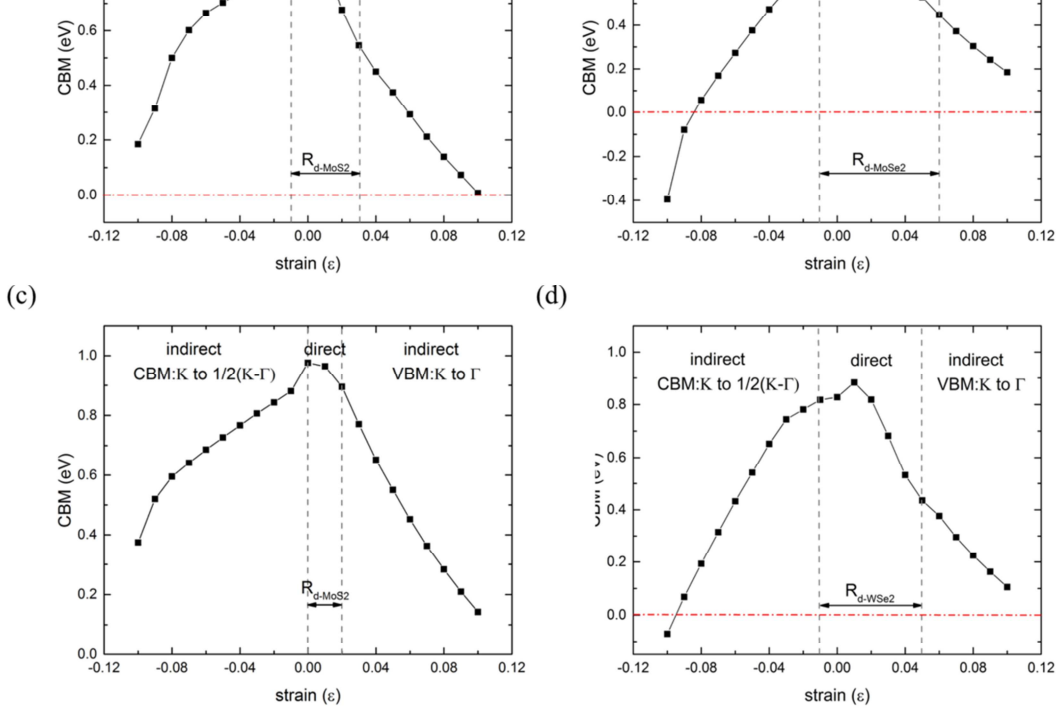

Figure 5. CBM variation of monolayer MoS_2 (a), $MoSe_2$ (b), WS_2 (c) and WSe_2 (d) with compressive and tensile symmetric strains.

As seen from Figure 6, we depict the spatial distribution of the charge density for the monolayer MoS_2, $MoSe_2$, WS_2 and WSe_2 under the strain-free state. All of four TMDs are formed by covalent bonding with four electrons from external shells of metal atoms being donated to the counterpart non-metal atoms. The binding energy (E) of these four materials are therefore predominately determined by the bond length (L) between adjacent atoms. Figure 7 shows that the calculated X-X bond length of monolayer MoS_2, $MoSe_2$, WS_2 and WSe_2 become closer due to Poisson contraction. The X-X bond lengths become smaller by about 0.024 Å, 0.025 Å, 0.023 Å and 0.021 Å per +1% biaxial strains for monolayer MoS2, MoSe2, WS_2 and WSe2, respectively. Moreover, the X-X bond length nearly decreases linearly with the deformation from -10% to +10%. Figure 7 shows a trend of L_{MoS2}<L_{WS2}< L_{MoSe2}<L_{WSe2} from -1% to +5% deformation, which is the the most deformation change width of direct band gap region of the CBM-strain curve in Figure 5. From this result, we can

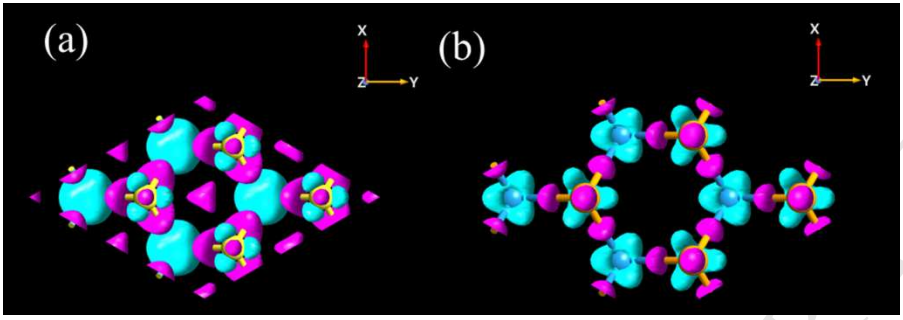

Figure 6. The isosurface plot of the charge density of monolayer MoS_2 and $MoSe_2$ (a), WSe_2 and WS_2 (b). The isosurface value was taken as 0.05 $e/Å^3$.

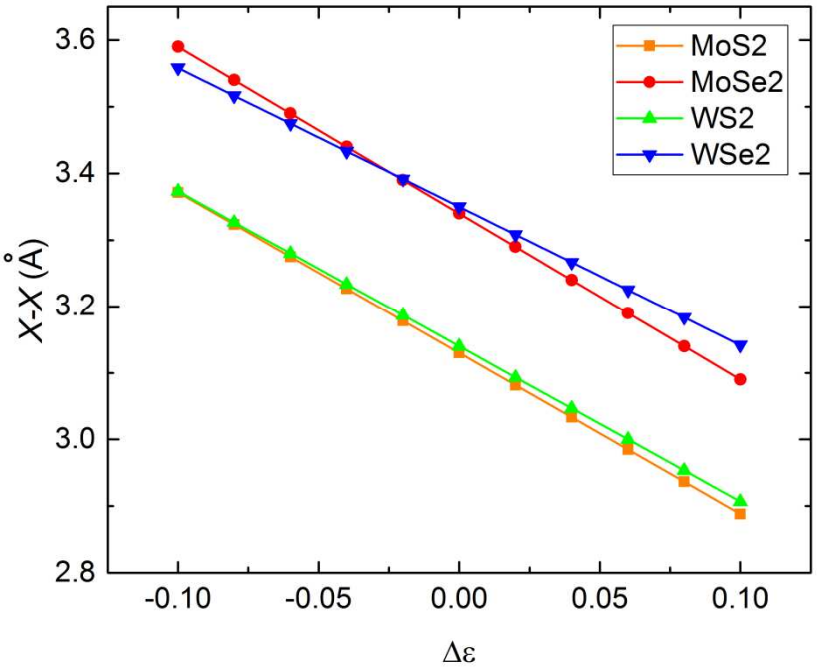

Figure 7. Evolution of the *X-X* bond length with respect to strains.

Young's modulus (*Y*) of all four TMDs (Y_{MoS2}, Y_{MoSe2}, Y_{WS2} and Y_{WSe2}) can be calculated using the first-principles methods[26, 29, 36]. Simulation results in Figure 8 shows that stress-strain curve firstly display a nonlinear characteristic, indicating Young's modulus has a

the bonding force (F) and the atomic separation (r), where, $F \propto 1/r^2$. By stretching the material, atomic separation increases, leading to reduced F, which is macroscopically reflected the reduced elastic modulus. The material softening of the monolayer MoS_2 has been reported previously in[29, 40]. Second, Figure 8 shows that in the small strain region (from -0.012 to 0.012), the elastic modulus for these materials are calculated to be Y_{MoS2}=217.6 GPa, Y_{MoSe2}=171.4 GPa, Y_{WS2}=218.8 and Y_{WSe2}=201.5 GPa, which demonstrate a trend of $Y_{WS2}>Y_{MoS2}>Y_{WSe2}>Y_{MoSe2}$.

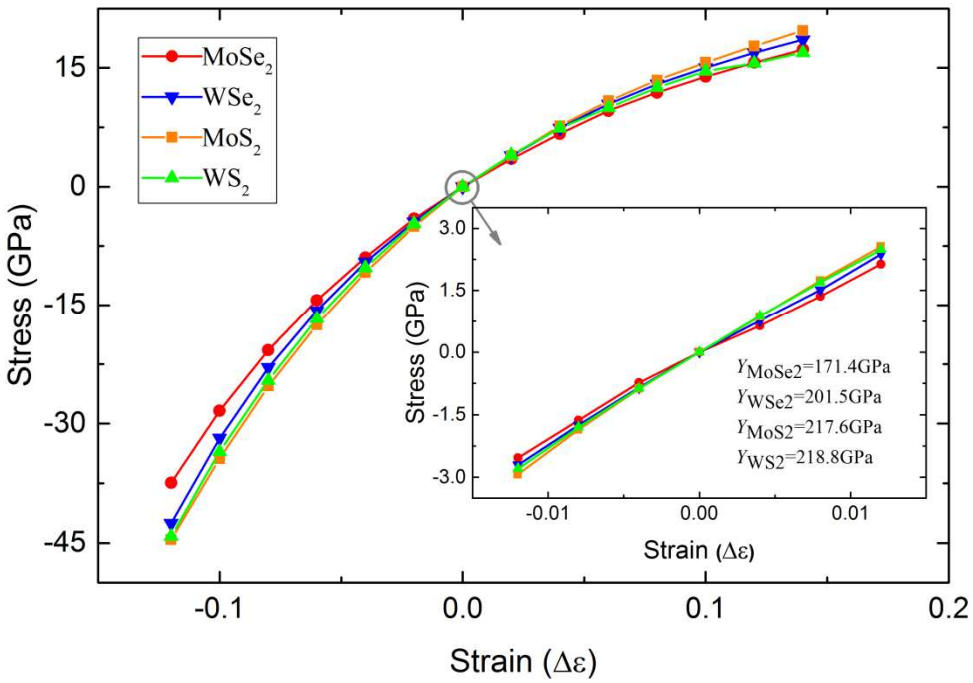

Figure 8. Stress-strain curve for monolayer MoS_2, $MoSe_2$, WS_2 and WSe_2.

Macroscopically the inter-atomic bonding force is reflected by the Young's modulus, characteristic of material stiffness defined as stress per unit strain. It is a logical elucidation that a higher Young's modulus leads to a higher inter-atomic bonding force, hence under an identical strain, the material that has a higher Young's modulus will experience a greater stress. For example, the Young's modulus of WS_2 is higher than MoS_2 than WSe_2 than $MoSe_2$ in Figure 8. Application of tensile strains on WS_2 decreases the S-S bong length. The effect is a reduction in the W-*d* orbital and S-*p* orbital coupling, which is revealed as the

demonstrates WS_2 has the lowest stability and resulting in the narrowest deformation region of the CBM-strain curve in Figure 5. Results from the above analysis and data of the Young's modulus, it is deduced that $E_{g\text{-}WS2} > E_{g\text{-}MoS2} > E_{g\text{-}WSe2} > E_{g\text{-}MoSe2}$ and $R_{d\text{-}WS2} < R_{d\text{-}MoS2} < R_{d\text{-}WSe2} < R_{d\text{-}MoSe2}$, which is exactly matching with the results from the first-principles simulations about the band gap and the direct band gap region. It can be concluded that a TX_2 having smaller young's modulus will be more immune to mechanical strains, exhibiting greater electro-mechanical stability.

Figure 9 and Figure 10 show the band structures evolution with the asymmetrical biaxial compressive and the tensile strains along the armchair (ε_a) and zigzag (ε_z) directions on the monolayer TX_2 orthorhombic cell. We investigate the CBM of the band due to strains in directions between ε_a and ε_z. Firstly, the simulation was conducted by setting the ε_a-direction strains to increase while keeping the ε_z unchanged. Then we repeat the calculation when ε_z-direction strains increases by a small step. In this way, the strains direction between ε_a- and ε_z- that leads to the most notable change of the CBM can be obtained. We define a total strains of $\varepsilon_t = \sqrt{{\varepsilon_a}^2 + {\varepsilon_z}^2}$. It is seen from the simulation results in the Figure 9 that for the compressive strains, the reduction of the CBM under ε_a-direction is faster than ε_z-direction. The ε_t threshold deformation of the CBM reaching to 0 eV are roughly 13%, 9% and 11% for monolayer MoS_2, $MoSe_2$ and WSe_2, respectively. The CBM declines more quickly under a pure ε_a- or ε_z- direction deformation than the deformations along the 45^o angle between ε_a- and ε_z- direction, which displays a strong directional dependence effect. However, Figure 10 shows for the tensile strains, the reduction of the CBM under uniaxial ε_a- or ε_z- direction is smaller than biaxial symmetrical deformation both in ε_a- and ε_z-direction. From Figure 10, it can be concluded that for the tensile strains, the ε_t threshold deformation for the CBM reaching to 0 eV are roughly 22.6%, 21.2% and 19.8% for monolayer MoS_2, $MoSe_2$ and WSe_2, respectively. For the tensile strains, the effect on the band structures is almost independent on the direction of the strains.

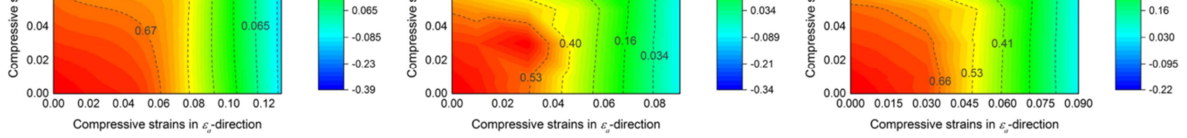

Figure 9. CBM variation of the monolayer MoS_2 (a), $MoSe_2$ (b) and WSe_2 (c) orthorhombic cell with compressive strains.

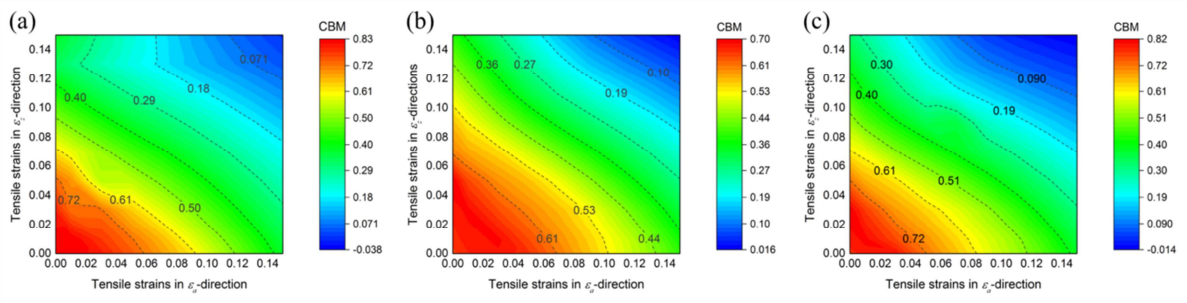

Figure 10. CBM variation of the monolayer MoS_2 (a), $MoSe_2$ (b) and WSe_2 (c) orthorhombic cell with tensile strains.

4 Conclusion

To summarize, the first-principles methods have been used to investigate the electronic and mechanical properties of four monolayer TMD materials - MoS_2, $MoSe_2$, WS_2 and WSe_2. Hexagonal and orthorhombic cell structures of all these materials have been built and subsequently simulated when subjecting to tensile and compressive strains. Main conclusion is deduced that the region of the direct band gap in the CBM-strain curves exhibiting a trend of $R_{\text{d-WS2}}<R_{\text{d-MoS2}}<R_{\text{d-WSe2}}<R_{\text{d-MoSe2}}$, which has been systematically underpinned by further first-principles studies on the stress-strain relation. In the Young's modulus and band gap study, it has been analyzed that the Young's modulus and band gap of these four materials demonstrate a pattern of $Y_{\text{WS2}}>Y_{\text{MoS2}}>Y_{\text{WSe2}}>Y_{\text{MoSe2}}$ and $E_{g\text{-WS2}}>E_{g\text{-MoS2}}>E_{g\text{-WSe2}}>E_{g\text{-MoSe2}}$. Therefore, it is reasonable to conclude that "softer" monolayer TX_2 have wider direct band gap regions and higher band gap, which is a desirable property for photoluminescence applications. Then, for the orthorhombic cell, the CBM declines more quickly under a pure ε_a or ε_z direction compressive strains than the strains in between ε_a and ε_z , which displays a strong directional dependence effect. However, the strains effect on the band structures is

Acknowledgement:

Authors would like to acknowledge China Scholarship Council for support.

References

[1] L.J. Li, Y. Zhang, Controlling the luminescence of monolayer MoS2 based on the piezoelectric effect, Nano Research, 10 (2017) 2527-2534.
[2] A. Surrente, D. Dumcenco, Z. Yang, A. Kuc, Y. Jing, T. Heine, Y.C. Kung, D.K. Maude, A. Kis, P. Plochocka, Defect Healing and Charge Transfer-Mediated Valley Polarization in MoS2/MoSe2/MoS2 Trilayer van der Waals Heterostructures, Nano Letters, 17 (2017) 4130-4136.
[3] Q.L. Xiong, J. Zhang, C. Xiao, Z.H. Li, Effects of atomic vacancies and temperature on the tensile properties of single-walled MoS2 nanotubes, Physical Chemistry Chemical Physics, 19 (2017) 19948-19958.
[4] K.D. Park, O. Khatib, V. Kravtsov, G. Clark, X.D. Xu, M.B. Raschke, Hybrid Tip-Enhanced Nanospectroscopy and Nanoimaging of Monolayer WSe2 with Local Strain Control, Nano Letters, 16 (2016) 2621-2627.
[5] R. Addou, S. McDonnell, D. Barrera, Z.B. Guo, A. Azcatl, J. Wang, H. Zhu, C.L. Hinkle, M. Quevedo-Lopez, H.N. Alshareef, L. Colombo, J.W.P. Hsu, R.M. Wallace, Impurities and Electronic Property Variations of Natural MoS2 Crystal Surfaces, ACS Nano, 9 (2015) 9124-9133.
[6] X.P. Fu, F.F. Li, J.F. Lin, Y.B. Gong, X.L. Huang, Y.P. Huang, B. Han, Q. Zhou, T. Cui, Pressure-Dependent Light Emission of Charged and Neutral Excitons in Monolayer MoSe2, J Phys Chem Lett, 8 (2017) 3556-3563.
[7] A.J. McKenna, J.K. Eliason, D.J. Flannigan, Spatiotemporal Evolution of Coherent Elastic Strain Waves in a Single MoS2 Flake, Nano Lett., 17 (2017) 3952-3958.
[8] Z.H. Yu, Y.M. Pan, Y.T. Shen, Z.L. Wang, Z.Y. Ong, T. Xu, R. Xin, L.J. Pan, B.G. Wang, L.T. Sun, J.L. Wang, G. Zhang, Y.W. Zhang, Y. Shi, X.R. Wang, Towards intrinsic charge transport in monolayer molybdenum disulfide by defect and interface engineering, Nature Communications, 5 (2014).
[9] K.F. Mak, C. Lee, J. Hone, J. Shan, T.F. Heinz, Atomically Thin MoS2: A New Direct-Gap Semiconductor, Phys. Rev. Lett., 105 (2010) 136805.
[10] H.R. Gutierrez, N. Perea-Lopez, A.L. Elias, A. Berkdemir, B. Wang, R. Lv, F. Lopez-Urias, V.H. Crespi, H. Terrones, M. Terrones, Extraordinary Room-Temperature Photoluminescence in Triangular WS2 Monolayers, Nano Letters, 13 (2013) 3447-3454.
[11] C.H. Chang, X.F. Fan, S.H. Lin, J.L. Kuo, Orbital analysis of electronic structure and phonon dispersion in MoS2, MoSe2, WS2, and WSe2 monolayers under strain, Physical Review B, 88 (2013) 195420.
[12] J.S. Ross, S.F. Wu, H.Y. Yu, N.J. Ghimire, A.M. Jones, G. Aivazian, J.Q. Yan, D.G. Mandrus, D. Xiao, W. Yao, X.D. Xu, Electrical control of neutral and charged excitons in a monolayer semiconductor, Nature Communications, 4 (2013).
[13] A. Ramasubramaniam, Large excitonic effects in monolayers of molybdenum and tungsten dichalcogenides, Phys. Rev. B, 86 (2012) 115409.

[16] S.F. Wu, J.S. Ross, G.B. Liu, G. Aivazian, A. Jones, Z.Y. Fei, W.G. Zhu, D. Xiao, W. Yao, D. Cobden, X.D. Xu, Electrical tuning of valley magnetic moment through symmetry control in bilayer MoS2, Nature Physics, 9 (2013) 149-153.
[17] G. Sallen, L. Bouet, X. Marie, G. Wang, C.R. Zhu, W.P. Han, Y. Lu, P.H. Tan, T. Amand, B.L. Liu, B. Urbaszek, Robust optical emission polarization in MoS2 monolayers through selective valley excitation, Physical Review B, 86 (2012) 081301.
[18] H.L. Zeng, J.F. Dai, W. Yao, D. Xiao, X.D. Cui, Valley polarization in MoS2 monolayers by optical pumping, Nature Nanotechnology, 7 (2012) 490-493.
[19] T. Cao, G. Wang, W.P. Han, H.Q. Ye, C.R. Zhu, J.R. Shi, Q. Niu, P.H. Tan, E. Wang, B.L. Liu, J. Feng, Valley-selective circular dichroism of monolayer molybdenum disulphide, Nature Communications, 3 (2012).
[20] F.F. Yu, Q.W. Liu, X. Gan, M.X. Hu, T.Y. Zhang, C. Li, F.Y. Kang, M. Terrones, R.T. Lv, Ultrasensitive Pressure Detection of Few-Layer MoS2, Adv. Mater., 29 (2017) 1603266.
[21] Y.H. Chang, W. Zhang, Y. Zhu, Y. Han, J. Pu, J.K. Chang, W.T. Hsu, J.K. Huang, C.L. Hsu, M.H. Chiu, T. Takenobu, H. Li, C.I. Wu, W.H. Chang, A.T.S. Wee, L.J. Li, Monolayer MoSe2 Grown by Chemical Vapor Deposition for Fast Photodetection, ACS Nano, 8 (2014) 8582-8590.
[22] K.F. Mak, K.L. McGill, J. Park, P.L. McEuen, The valley Hall effect in MoS2 transistors, Science, 344 (2014) 1489-1492.
[23] C.V. Nguyen, V.V. Ilyasov, H.V. Nguyen, H.N. Nguyen, Band gap and electronic properties of molybdenum disulphide under strain engineering: density functional theory calculations, Mol. Simulat., 43 (2017) 86-91.
[24] M.G. Sensoy, D. Vinichenko, W. Chen, C.M. Friend, E. Kaxiras, Strain effects on the behavior of isolated and paired sulfur vacancy defects in monolayer MoS2, Physical Review B, 95 (2017) 014106.
[25] P. Lu, X.J. Wu, W.L. Guo, X.C. Zeng, Strain-dependent electronic and magnetic properties of MoS2 monolayer, bilayer, nanoribbons and nanotubes, Physical Chemistry Chemical Physics, 14 (2012) 13035-13040.
[26] M. Ghorbani-Asl, S. Borini, A. Kuc, T. Heine, Strain-dependent modulation of conductivity in single-layer transition-metal dichalcogenides, Physical Review B, 87 (2013) 235434.
[27] E. Scalise, M. Houssa, G. Pourtois, V.V. Afanas'ev, A. Stesmans, Strain-induced semiconductor to metal transition in the two-dimensional honeycomb structure of MoS2, Nano Research, 5 (2012) 43-48.
[28] K. He, C. Poole, K.F. Mak, J. Shan, Experimental Demonstration of Continuous Electronic Structure Tuning via Strain in Atomically Thin MoS2, Nano Lett., 13 (2013) 2931-2936.
[29] T.S. Li, Ideal strength and phonon instability in single-layer MoS2, Physical Review B, 85 (2012) 235407.
[30] S.V. Bondarchuk, B.F. Minaev, Two isomeric solid carbon nitrides with 1:1 stoichiometry which exhibit strong mechanical anisotropy, New J Chem, 41 (2017) 13140-13148.
[31] S.V. Bondarchuk, B.F. Minaev, Two-dimensional honeycomb (A7) and zigzag sheet (ZS) type nitrogen monolayers. A first principles study of structural, electronic, spectral, and mechanical properties, Comp Mater Sci, 133 (2017) 122-129.

[34] J.P. Perdew, K. Burke, M. Ernzerhof, Generalized gradient approximation made simple, Phys. Rev. Lett., 77 (1996) 3865-3868.
[35] D. Saha, S. Mahapatra, Atomistic modeling of the metallic-to-semiconducting phase boundaries in monolayer MoS2, Appl. Phys. Lett., 108 (2016) 253106.
[36] Q.Y. Zhang, Y.C. Cheng, L.Y. Gan, U. Schwingenschlogl, Giant valley drifts in uniaxially strained monolayer MoS2, Physical Review B, 88 (2013) 245447.
[37] S. Horzum, H. Sahin, S. Cahangirov, P. Cudazzo, A. Rubio, T. Serin, F.M. Peeters, Phonon softening and direct to indirect band gap crossover in strained single-layer MoSe2, Physical Review B, 87 (2013) 125415.
[38] C. Ataca, S. Ciraci, Functionalization of Single-Layer MoS2 Honeycomb Structures, J Phys Chem C, 115 (2011) 13303-13311.
[39] A. Kuc, N. Zibouche, T. Heine, Influence of quantum confinement on the electronic structure of the transition metal sulfide TS2, Physical Review B, 83 (2011) 245213.
[40] R.C. Cooper, C. Lee, C.A. Marianetti, X.D. Wei, J. Hone, J.W. Kysar, Nonlinear elastic behavior of two-dimensional molybdenum disulfide (vol 87, 035423, 2013), Physical Review B, 88 (2013) 039906.

effect to the compressive strain.